Applied Catalysis B: Environmental 154–155 (2014) 350–359

Contents lists available at ScienceDirect

Applied Catalysis B: Environmental

journal homepage: www.elsevier.com/locate/apcatb

Abatement of organics and *Escherichia coli* using CeO_2-TiO_2 composite oxides: Ultraviolet and visible light performances

Mario J. Muñoz-Batista, Manuel Ferrer, Marcos Fernández-García, Anna Kubacka*

Instituto de Catálisis y Petroleoquímica, CSIC, Marie Curie 2, 28049 Madrid, Spain

ARTICLE INFO

Article history:
Received 7 January 2014
Received in revised form 16 February 2014
Accepted 19 February 2014
Available online 4 March 2014

Keywords:
Photo-catalysis
Mineralization
Disinfection
Germicide
UV
Sunlight
Titania
Ceria

ABSTRACT

A series of CeO_2-TiO_2 composite samples were obtained by a single-pot microemulsion method followed by calcination. The composite samples contain fluorite (CeO_2) and anatase (TiO_2) nanometric phases with a ceria content ranging from 1 to 25 mol%. Using these samples as photocatalysts, toluene mineralization and *Escherichia coli* 1337-H inactivation were carried out under UV and visible illumination conditions. To interpret the photo-catalytic results and provide quantitative bases to compare the performance of the composite samples with respect to titania and ceria single oxide nano-references the study focuses on analyzing kinetic differences. The kinetic analysis of both types of degradation processes provides conclusive evidence that the composite Ce-Ti system outperforms the Ti reference nano-materials (including P25) by a factor exceeding 3 under UV conditions and 1.7 for sunlight-type or visible light. Together with the low activity of the Ce single reference, the results show that a synergistic effect occurs between the two oxide components of the Ce-Ti system. Maximum activity, irrespective of the chemical or biological target nature as well as the energy of the excitation, was always achieved with samples having low Ce loadings, below 5 mol%. Such a general enhanced activity indicates that the Ce-Ti system can be a "universal" candidate to provide a highly active material with improved performance with respect to nano-anatase.

1. Introduction

Heterogeneous photocatalysis is an Advanced Oxidation Process using nanocrystalline semiconductors which find useful utilization in the degradation of both organic and biological pollutants. This is essentially based in the excellent performance and stability of titania, one of the most prominent photocatalytic material for the mineralization of typical pollutants as organic molecules or the inactivation of microorganisms that can pose serious health, food or other risks. Its action is typically carried out under mild conditions, e.g. room temperature and atmospheric pressure and using oxygen (air) as oxidant agent [1–7]. Anatase, the stable nanopolymorph of titania [4], is among the most active photo-materials largely because it shows a correct balance between its surface chemistry-related properties and the adequate physical properties for efficient handling of light-triggered charge carriers, allowing them to be involved in chemical/biological steps at the surface [4–7]. The quest of improving anatase photo-degradation properties was however pursued almost from the beginning of the photocatalytic field. Several strategies were tested, being most popular ones in the case of organic pollutants related to the electronic modification of titania through cationic [1,2,4,8,9], anionic [1,2,4,10], and anionic-cationic [2,4,11–17] (co)-doping. This path has been relatively less utilized in the case of biological photo-inactivation [18,19]. For both biological and chemical degradation reactions the use of a visible-light-sensitize phase in intimate contact with TiO_2 has been also considered [2,4–7,20–41].

In this work we aim to explore the chemical potential of the CeO_2-TiO_2 oxide-oxide heterojunction upon both UV and Visible light excitation. The CeO_2-TiO_2 system is known to provide rather active materials independently of the excitation wavelength [4,42]. It has been applied for the elimination of organic pollutants through reduction and/or oxidation reactions [43–50] and, very recently, for the inactivation of microorganisms [49]. Although ceria can have activity by itself [51–54] it is usually very limited as compared with titania. The CeO_2-TiO_2 composite system boosts this activity by a synergistic action between components. We previously analyzed such synergistic action under UV excitation and provided support to the interpretation that activity is connected to the production of holes able to generate chemistry at the surface of the material and this, in turn, appeared directly linked to the beneficial effect

* Corresponding authors. Fax: +34 915854760.
E-mail addresses: m.fernandez@icp.csic.es, mfg@icp.csic.es (M. Fernández-García), ak@icp.csic.es (A. Kubacka).

http://dx.doi.org/10.1016/j.apcatb.2014.02.038
0926-3373/

Nomenclature

Rate	reaction rate, mol m^{-2} s^{-1}
n	inverse of number of charge carrier, dimensionless
γ	quantum efficiency correcting factor, dimensionless
S	fractional selectivity, dimensionless
$e^{a,s}$	local rate of photon absorption, Einstein cm^{-2} s^{-1}
I	lamp radiation intensity, Einstein cm^{-2} s^{-1} sr^{-1}
K	spectral absorption coefficients, dimensionless
e	thickness, cm
x,y,z	cartesian coordinate, cm
φ,θ	spherical coordinate, rad
n_G	outwardly directed (to the catalytic film) unit normal vector, dimensionless
Ω	solid angle, sr
Ω	unit vector in the direction of radiation propagation, dimensionless
β	angle between the ray trajectory and the film outwardly directed normal, rad
λ	wavelength, nm
a,b	x,y cartesian components of the outwardly directed normal vector, dimensionless
R	radius of sample cylinder, cm
RL	lamp radius, cm
N	microorganism concentration, CFU ml^{-1}
k	kinetic constant for microorganism inactivation, CFU ml^{-1} min^{-1}
K	pseudo-adsorption constants for microorganism inactivation, (CFU ml^{-1} $)^n$

Subscripts

i	relative to i product
g	relative to glass
s	relative to the sample film
max	maximum limiting value
min	minimum limiting value
L	relative to lamp
s	relative to the sample film
Lm	relative to the surface lamp
u	relative to undamaged microorganisms
d	relative to damaged microorganisms

Superscripts

n	inhibition coefficient for microorganism inactivation, dimensionless

exerted at charge recombination by ceria oxygen vacancies specifically generated at the ceria-anatase oxide interface [50]. The last phenomenon has an acute size-dependence of the ceria particle component as evidenced by the corresponding size-dependence of the redox properties of the oxide [55].

In this contribution we plan to test the photo-catalytic role of the CeO_2-TiO_2 interface as a function of the CeO_2 content of the material, paying particular attention to examine the behavior of the system upon both UV and Sunlight-type excitations. Previously we characterized thoroughly the system as a function of the Ce oxide content using a multitechnique approach [50]. Instead of focusing in obtaining structure-activity links, here we try to obtain photo-catalytic data in toluene photo-elimination as well as in the inactivation of a model health and food risk-associated bacterium, *Escherichia coli* strain 1337-H.

To this end, we subjected the photo-catalytic results concerning toluene photo-degradation and *E. coli* inactivation to kinetic analysis and report results which would allow the comparison among samples on quantitative basis. More concretely, we obtained the kinetic constants of the two photo-processes tested and, in the case or the organic pollutant degradation, due to the relatively well known chemistry of the mineralization process, we obtained a real estimation of the quantum efficiency. For the analysis of the microorganism inactivation, Marugán et al. [56] developed a powerful method to analyze intrinsic kinetics using the calculation of the local superficial rate of photon absorption ($e^{a,s}$). Here we did not apply such method for two main reasons; first, the light–matter interaction in liquid phase does not have a time-independent or easily defined interaction interface, which makes complex the analysis of optical (and particularly scattering) properties [57]. In the case of organic depollution processes, the situation is much clear (see ref. [58] as an illustrative example directly related to this work). More importantly, the second limit considers the fact that we do not know the exact chemical nature of the catalyst–microorganism interaction and thus cannot provide accurate measurements of the quantum efficiency, as we will do for the elimination of toluene. Differences in the chemical stages of the interaction of the samples with the microorganisms are too complex to be studied and have not been fully elucidated up to date in the literature [5–7]. Therefore, for our specific situation we will compare the inactivation performance of the Ce-Ti samples in terms of the kinetic constants obtained by the kinetic analysis of the inactivation curves [41].

The analysis performed in this contribution indicates that the most active Ce-Ti samples contains very low quantities of CeO_2 for both UV and sunlight-type excitation, irrespective of the target nature, chemical or biological. This demonstrates the general usefulness of the CeO_2-TiO_2 system independently of the process nature and conditions.

2. Experimental

2.1. Catalyst preparation

Materials were obtained by means of a microemulsion preparation method utilizing *n*-heptane (Scharlau) as organic media, Triton X-100 (Aldrich) as surfactant and hexanol (Aldrich) as cosurfactant. A TiO_2 reference sample was obtained as a first step using a water in oil microemulsion and titanium tetraisopropoxide as precursor. In all composite samples and the CeO_2 reference, cerium nitrate (Alfa Aesar) was introduced in the aqueous phase of a microemulsion. After stirring for 30 min, the stoichoimetric (to obtain the corresponding Ce(III) hydroxide) quantity of tetramethylammonium-hydroxide (TMAH) was introduced from the aqueous phase of a similar microemulsion under stirring for ca. 5 min. For nanocomposite samples, a titanium tetraisopropoxide solution with isopropanol (2:3) was added dropwise on the Ce-containing microemulsion. Water/M (M = Ti, Ce, or Ce + Ti) and water/surfactant molar ratios were, respectively, 110 and 18 for all samples [59,60]. The resulting mixture was stirred for 24 h, centrifuged, and the separated solid precursors rinsed with methanol and dried at 110 °C for 12 h. After drying, the solid precursors were subjected to a heating ramp (2 °C min^{-1}) up to 500 °C, maintaining this temperature for 2 h. Samples names are Ti/Ce for titania-TiO_2/ceria-CeO_2 reference materials, and xCeTi for the composite ones where x is the molar content of CeO_2 (in relation to a fixed amount of titania corresponding to 1 mol).

2.2. Photo-catalytic degradation of toluene

Gas phase selective photo-oxidation tests were carried out with toluene and using a set-up described elsewhere [58]. Activity and selectivity for the gas-phase photooxidation were tested in a

continuous flow annular photoreactor containing ca. 40 mg of photocatalyst as a thin layer coating on a pyrex tube. The corresponding amount of catalyst was suspended in 1 ml of ethanol, painted on a pyrex tube (cut off at ca. 290 nm) and dried at room temperature (R.T.). The reacting mixture (100 ml/min) was prepared by injecting styrene (≥99%; Aldrich) into a wet (ca. 75% relative humidity, RH) 20 vol.% O_2/N_2 flow before entering to the photoreactor, yielding an organic inlet concentration of ca. 700 ppmv. Under such conditions, the reaction rate shows a zero order kinetics with respect to the total flow and organic pollutant/oxygen concentrations. After flowing the mixture for 6 h (control test) in the dark, the catalyst was irradiated by four fluorescent daylight lamps (6 W, Sylvania F6 W/D) with a radiation spectrum simulating sunlight (UV content of 3%; main emission lines at 410, 440, 540, and 580 nm), symmetrically positioned outside the photoreactor. Similar tests were carried out in selected samples using UV lamps (Sylvania F6WBLT-65; 6W, maximum at ca. 350 nm). A full description of the experimental set-up and illumination details is presented in Appendix A.

Reaction rates were evaluated under steady state conditions, typically achieved after ca. 8–10 h from the irradiation starting. No change in activity was detected for all samples within the next 12 h. The concentration of reactants and products was analyzed using an on-line gas chromatograph (Agilent GC 6890) equipped with HP-PLOT-Q/HP-Innowax columns (0.5/0.32 mm I.D. × 30 m) and TCD (for CO_2 measurement)/FID (organic measurement) detectors. Carbon balance was achieved in the 96–100% range in all experiments.

2.3. Quantum efficiency

The classical formulation of the quantum efficiency requires the calculation of the ratio between the number of molecules reacting by the number of photons interacting with the catalyst [61]:

$$\mathrm{QE}\% = \frac{\mathrm{Rate(mol\ m^{-2}s^{-1})}}{\mathrm{Photon\,Rate(Einstein\ m^{-2}\,s^{-1})}} \times 100 \quad (1)$$

To evaluate the denominator of equation (1), we first evaluate the local net superficial rate of photon absorption, $e^{a,s}$, of the samples. The mathematical expression and modeling of the present sample-reactor system allowing such calculation is presented in Appendix A. Once $e^{a,s}$ is obtained in the desired units (equation (1)) we need to consider the selectivity of the reaction as two different molecules are obtained in the toluene photo-oxidation reaction. A general equation for the quantum efficiency would be obtained using a correcting factor (here called γ) of the $e^{a,s}$ as follows:

$$\gamma_{\mathrm{TOL}} = \sum_i n_i S_i \quad (2)$$

Where i runs over all products of the reaction, S_i is the fractional selectivity to product i, and n_i is the inverse of number of charge carrier species required to obtain the specific i product. This correction factor accounts for the number of carge carrier species (and in turn photons) necessary to produce one molecule of a specific product and requires the measurement of the reaction selectivity. This is possible in the case of toluene photo-oxidation due to both the relatively well established mechanism as well as the limited number of intermediates detected in a gas-phase experiment [50,58,62].

2.4. Photo-catalytic inactivation of E. coli

The microorganism used in this study is *E. coli* 1337-H and was obtained from the German Collection of Microorganisms and Cell Cultures (DSMZ, Braunschweig, Germany) and cultured and maintained according to the recommendations of the suppliers [63]. Briefly, *E. coli* 1337-H was grown in Luria-Bertani (LB) medium at 37 °C using 100 mL flasks filled with 10 mL of the medium and subsequently used for photochemical cell viability assays. To study the antibacterial activity of the samples, a suspension containing 10 μL of microbial cells (ca. 8.8×10^9 cell forming units (CFU) mL^{-1}) suspended in 1 mL broth solution was made [64]. Aliquots of 1 mL from these suspensions were added to a 3 mL quartz cubic cell containing 1 mL of sterilized water and the corresponding powder under continuous stirring and oxygen supply. The slurry (at a previously optimized concentration of 0.6 g L^{-1}) was placed in the UV spectrometer chamber (Synergy HT Multi-Mode Microplate Reader - BioTek) and irradiated with a light at 350 (UV) and 500 (visible) nm for different time periods. The excitation linewidth is lower than 20 nm in all cases.

The xCeTi samples together with blank tests (using either light without catalyst or the materials at dark conditions) were measured using the same bacterium inoculums (8.8×10^9 CFU mL^{-1}). As demonstrated by blank experiments, care was put of using a sub-lethal, maximum radiation energy fluence of ca. 1.5 kJ m^{-2} throughout the study. Excitation was carried out with a UV-visible spectrometer (UVIKON 930) equipped with filters to obtain monochromatic radiation (±20 nm half width). After irradiation and for different time intervals, aliquots of 100 μL were transferred to a 10 mL LB broth test tube. The order of cell dilution at this stage was 10^{-2}. Loss of viability after each exposure time was determined by the viable count procedure on LB agar plates after serial dilution (10^{-2}–10^{-5}). All plates were incubated at 37 °C for 24 h after which they were scanned using a Bio-Rad Imaging System equipped with Analysis Software 4.6.5 (Bio-Rad) to enable enumeration of bacterial colonies among replicates. Detection limit of the automated method is below 5 colony units. Data reported in this contribution are typically the average of four different experiments. A minimum of four experimental runs was performed to determine antimicrobial activity.

2.5. Kinetic modelling

Modelling of the inactivation profiles was achieved, as mentioned, using an approach grounded in a simplified (Langmuir-Hinshelwood-like multistep-type) reaction mechanism based in three parameters; kinetic (k) and pseudo-adsorption (K) constants and an inhibition coefficient (n) [65]. The model considers that microorganism death occurs via a sequential attack of photo-radicals by which "undamaged" (denoted as u in subsequent equations) cells become "damaged" (denoted as d) and eventually progress to an "inactivated" state [65]. This leads to two differential equations as:

$$\frac{dN_u}{dt} = -k\frac{KN_u^n}{1+KN_u^n} \quad (3)$$

$$\frac{dN_d}{dt} = k\frac{KN_u^n - KN_d^n}{1+KN_u^n+KN_d^n} \quad (4)$$

We modified this model by assuming a fast decay from "undamaged" to inactivated cells which would lead to a simplified mechanism with a single differential equation paralleling the one of a classical Langmuir–Hinshelwood mechanism:

$$\frac{dN_u}{dt} = -k\frac{KN_u^n}{1+KN_u^n} \quad (5)$$

Numerical solution of the corresponding set of equations was achieved with a 5th order "adaptive size controlled" Runge-Kutta program, coupled to a Full Newton (non-linear fitting) algorithm [66]. Results reported here, e.g. in the specific reaction conditions used, concern the second model (single differential equation) as a better fit is obtained as judged by the coefficient of determination R^2. Note nonetheless the trends among the catalysts series using both models were the same, indicating that interpretation of the results are independent of the model.

3. Results and discussion

The physico-chemical characterization results for the xCeTi samples are summarized in Table 1. The system is composed by ceria (fluorite; *Fm3m* space group) and anatase ($I4_1/amd$ space group) nanoparticles with growing particle size (with Ce loading) in the case of ceria and a modest increasing trend for anatase. The study of the morphological properties indicates that ceria is

Table 1
Sample chemical composition and morphological properties.[a]

Sample	Ce/Ti TXRF	BET surface area ($m^2\ g^{-1}$)	Pore size (nm)	Porosity (%)	Anatase size (nm)	Fluorite size (nm)
Ti	–	113.5	8.31	47.9	12.1	–
0.01CeTi	0.02	83.5	6.17	35.0	13.0	–
0.025CeTi	0.03	78.0	6.12	35.7	13.2	–
0.05CeTi	0.06	75.5	6.83	34.4	15.0	5.3
0.1CeTi	0.12	77.2	4.60	27.2	15.0	9.4
0.25CeTi	0.30	108.8	5.39	42.6	15.2	8.5
Ce	–	101.0	–	–	–	8.5

[a] Standard error; Ce/Ti 0.01; BET 1.5 $m^2\ g^{-1}$; Porosity: 8%; Size 0.5 nm.

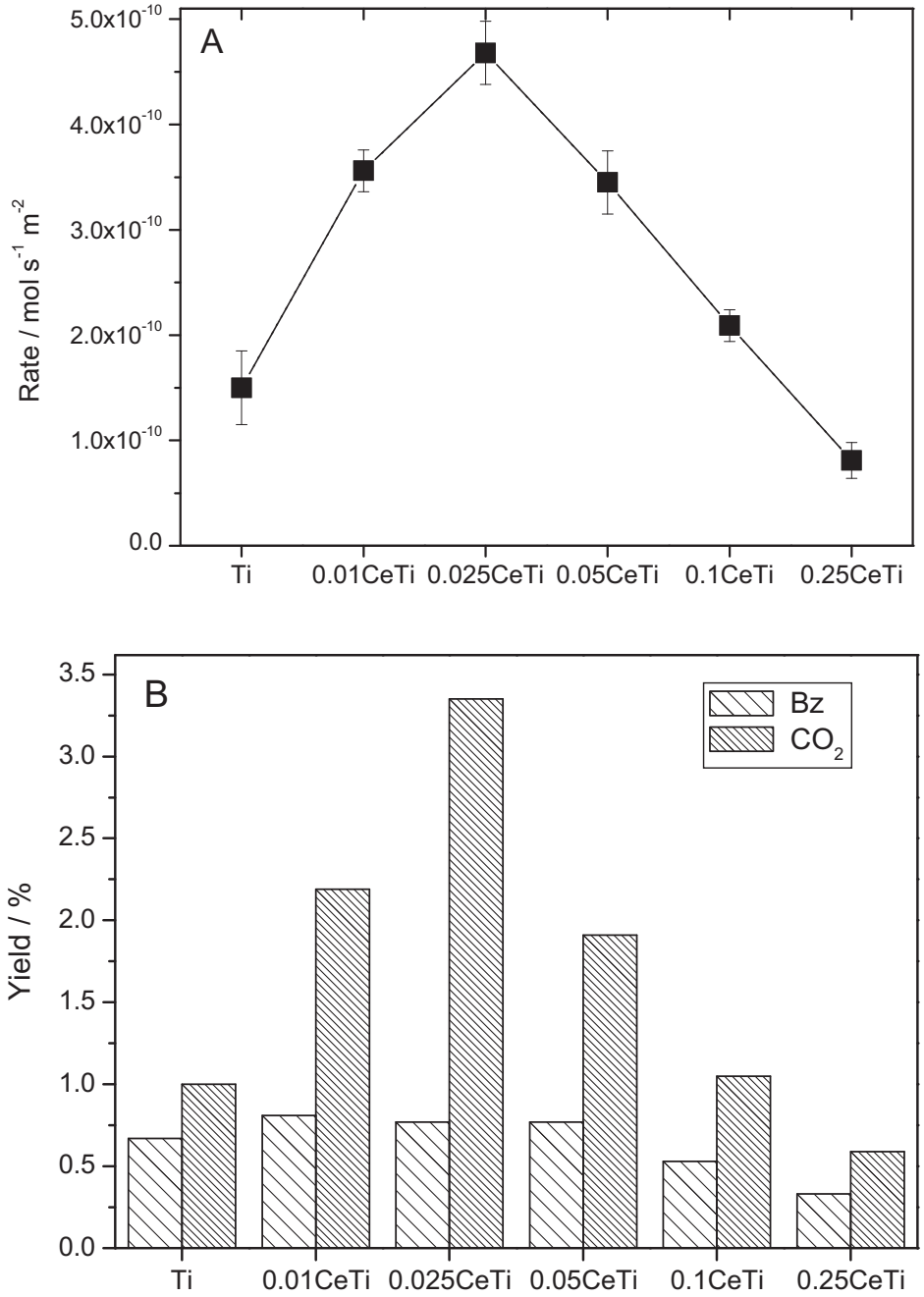

Fig. 1. Toluene photo-oxidation under UV irradiation. (A) Reaction rate; (B) yield. Yield is provided with a standard error of ±10%.

strongly interacting with the anatase phase up to a point close to the 0.1CeTi sample, likely penetrating the pores of the major phase (anatase). For this sample and samples with higher Ce loading, the presence of ceria nanoparticles of ca. 8–10 nm having loose contact with anatase are additionally observed [50].

The photo-chemical properties of the materials under UV and sunlight-type are presented in Figs. 1 and 2, respectively. The reaction rates as a function of the sample Ce content present an inverse U shape in both cases. A maximum is always obtained for xCeTi composite samples although the sample providing it is not the same; under UV corresponds to the 0.025CeTi (enhancement factor 3.4 with respect to Ti reference) while for sunlight-type excitation such maximum occurs for the 0.05CeTi sample (enhancement factor 1.7 with respect to the Ti reference). Note than the enhancement factors are larger with respect to the P25 (Evonik) reference, as stated previously [50]. For the two illumination conditions here tested all samples up to the 0.1CeTi display higher reaction rates than the Ti and Ce reference systems. The larger activity of relatively low Ce loaded samples in agreement with almost all previous reports concerning the Ce-Ti system [43–50].

Figs. 1 and 2 also contain selectivity data in panel B. As mentioned, toluene gas-phase photo-oxidation is relatively simple, yielding only two products, benzaldehyde and carbon dioxide. Independently of the simplicity, toluene is one of the most characteristic organic pollutants present in urban atmospheres and its elimination appears as a very stringent test to calibrate the performance of any photo-catalytic system [9,50,67]. For the xCeTi samples, the selectivity of the reaction varies as a function of the Ce content of the composite samples. Under UV a consistent increase to the total oxidation product, CO_2, is observed for samples up to the 0.1CeTi, with maximum for the 0.025CeTi specimen. Under sunlight-type illumination, the number of samples improving TiO_2 selectivity to CO_2 is lower, and this is only observed for the 0.025CeTi and 0.05CeTi samples.

As mentioned previously, the first step in calculating quantitative quantum efficiencies corresponds to the numerical calculation

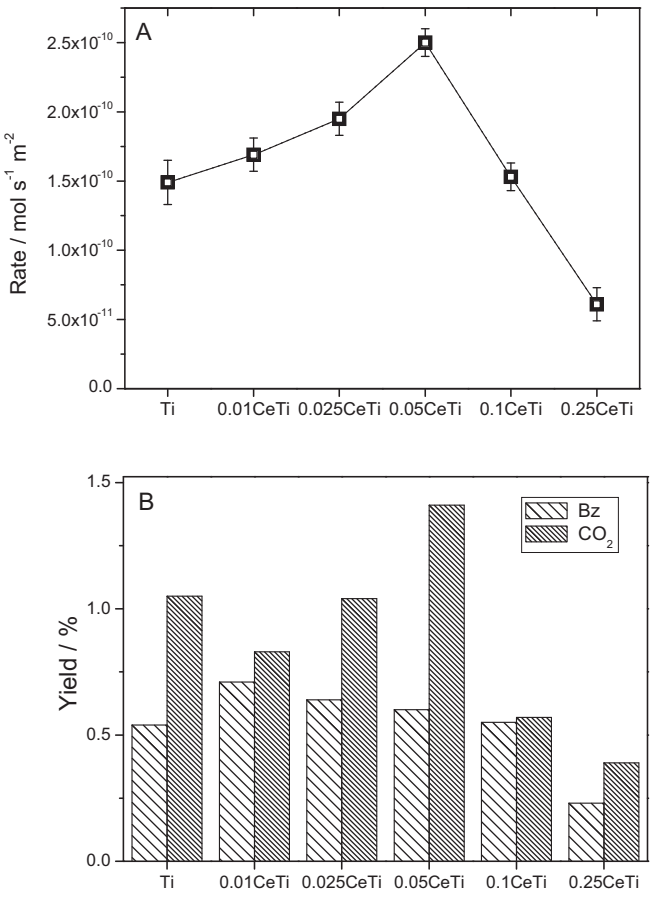

Fig. 2. Toluene photo-oxidation under Sunlight-type irradiation. (A) Reaction rate; (B) yield. Yield is provided with a standard error of ±10%.

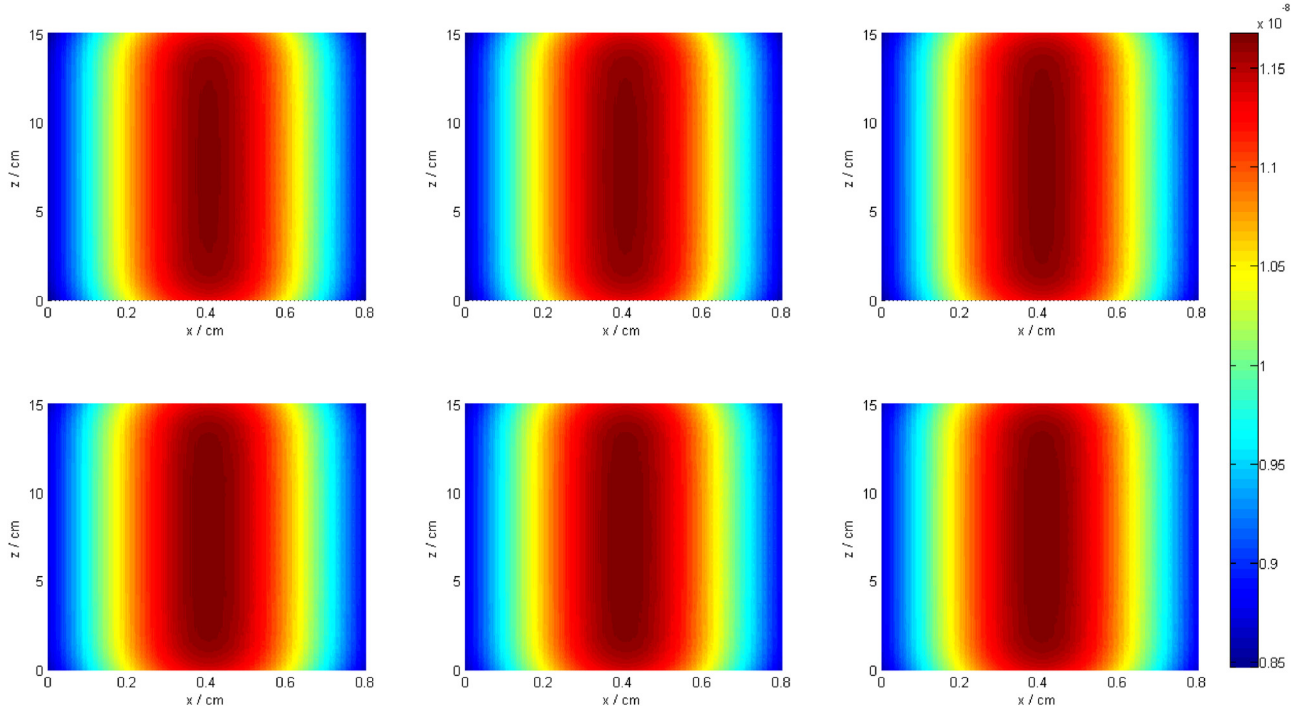

Fig. 3. Local rate of photon absorption (Einstein cm^{-2} s^{-1}) of the samples under UV irradiation. From right to left; upper row: Ti; 0.01CeTi and 0.025CeTi; lower row: 0.05CeTi, 0.1CeTi and 0.25CeTi.

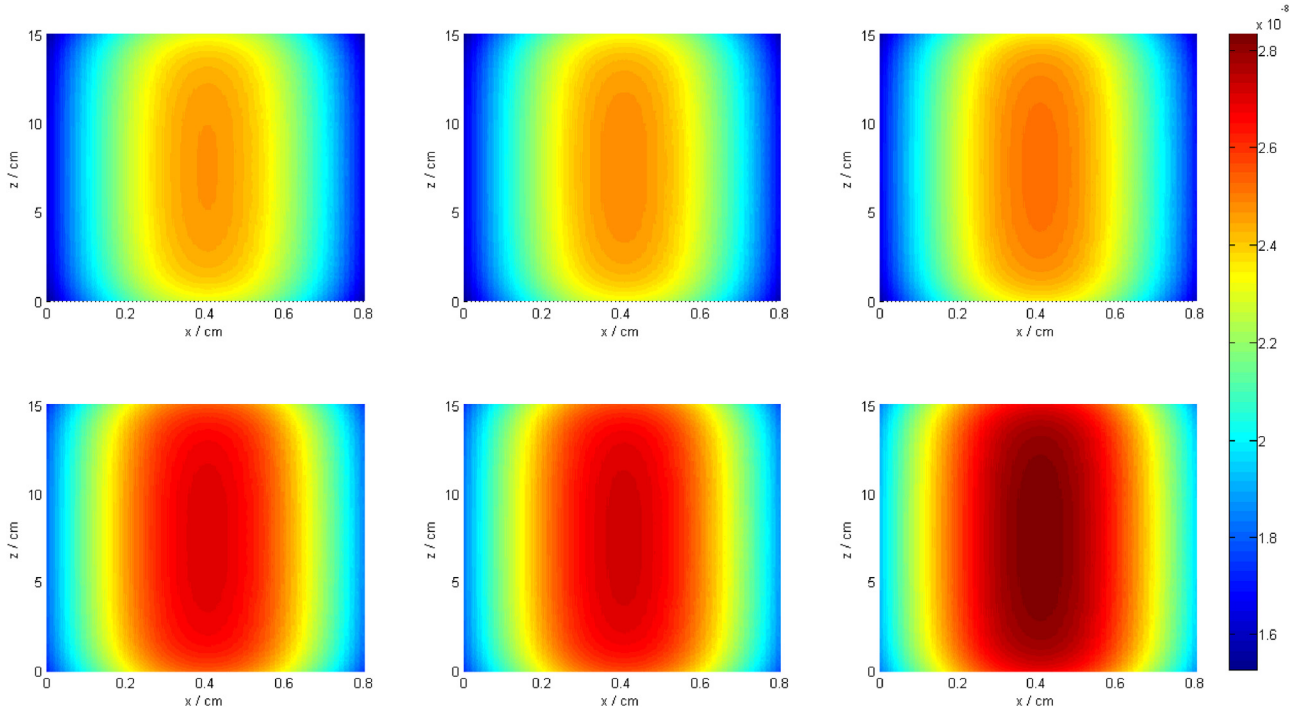

Fig. 4. Local rate of photon absorption (Einstein $cm^{-2}\ s^{-1}$) of the samples under Sunlight-type irradiation. From right to left; upper row: Ti; 0.01CeTi and 0.025CeTi; lower row: 0.05CeTi, 0.1CeTi and 0.25CeTi.

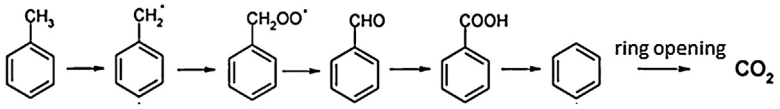

Scheme 1. Simplied reaction mechanism for toluene photo-oxidation.

of the local net superficial rate of photon absorption ($e^{a,s}$) at the sample surface. In our set-up (Appendix A) this requires the calculation on a cylindrical geometry and thus two independent geometrical variables are needed. This is presented in Fig. 3 (UV) and Fig. 4 (Sunlight-type) in Cartesian coordinates. The value of the $e^{a,s}$ observable is reasonably constant for UV while a larger variation (account up to 20% with respect to the Ti reference) is observed under Sunlight-type excitation. The geometrical (x,z) variation of the $e^{a,s}$ coefficient is rather similar for all samples and thus the differences among catalysts can be represented by the (surface) average value of the $e^{a,s}$ observable. The second factor to be considered is the one related to equation (2). This requires the selectivity data from Figs. 1 and 2 as well as the constant values n for benzaldehyde and CO_2. For the former we can count hole-related species for the initial steps leading to benzaldehyde (Scheme 1). In this case, it is well known that only one charge carrier species is required to provide the radical species presented at the first stage depicted in Scheme 1. In presence of (molecular) oxygen, such intermediate evolves in the desired product [50,58,62,68,69]. For the production of CO_2 the situation is less clear but, on average, four hole-related species (and corresponding $O_2^{\bullet-}$ species) are required [62,68,69]. The ratio between the number of charge carrier species used for CO_2 and benzaldehyde production is in any case the important parameter.

The calculation of the quantum efficiency (Q.E.) yielded values presented in Fig. 5. First to note is that the Q.E. values are rather small, always below 10^{-3}. A simple calculation of the so-called photonic efficiency following a standard recipe [34] provides about 2 orders of magnitude differences in values. This seems the general case observed in photo-catalytic systems [70]. The main, significant difference between the two calculations are not on the values but the relative (from one sample to other) error originated by neglecting the variation of $e^{a,s}$ and selectivity throughout the sample series (see below). In any case, focusing in Fig. 5 results, we can note that the quantum efficiency is on average ca. 5–6 times higher for UV than sunlight-type excitation; this factor in fact goes from ca. 2 for the Ti reference to ca. 7 for the 0.025CeTi sample. As the $e^{a,s}$ coefficient is only rather modesty varying through the

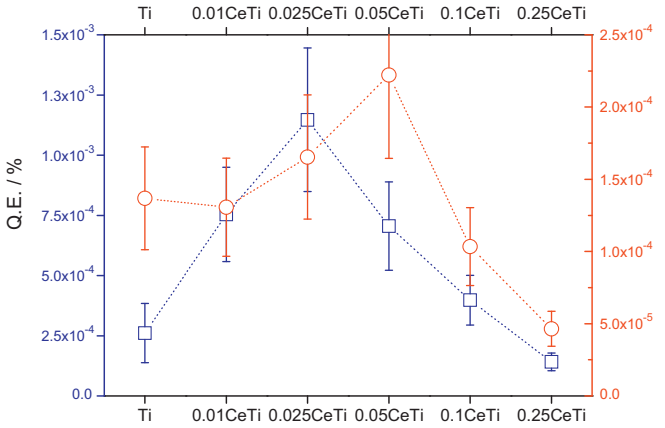

Fig. 5. Quantum efficiency of the toluene photo-oxidation reaction unver UV (blue) and Sunlight-type (red) irradation. (For interpretation of the color information in this figure legend, the reader is referred to the web version of the article.)

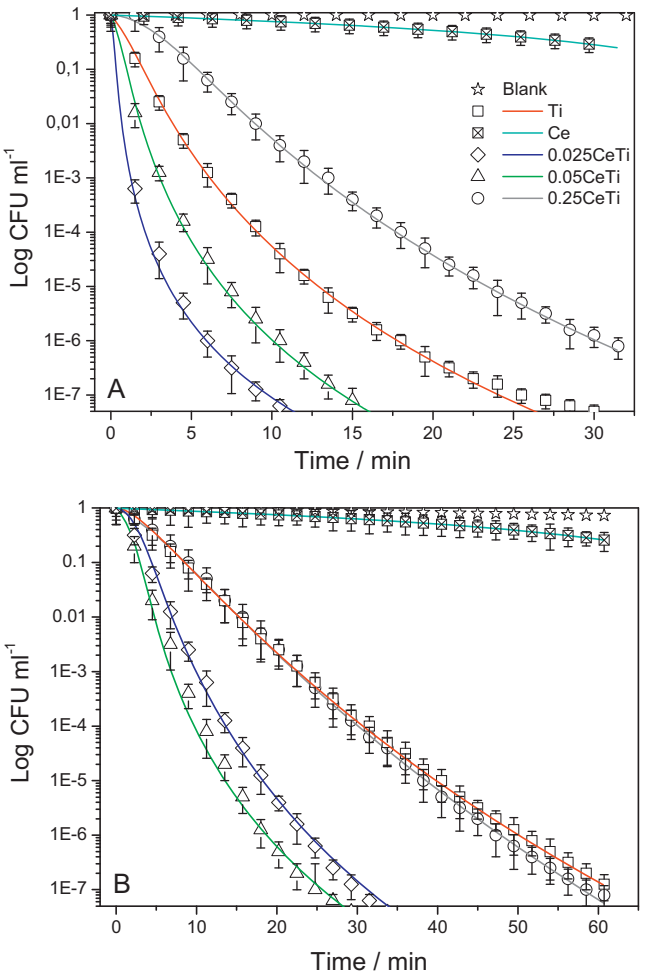

Fig. 6. Inactivation profiles (scattered data) and kinetic modelling (full lines) for *E. coli* bacterium under; (A) UV and (B) Visible light excitation. Color codes and symbols are defined in the upper panel.

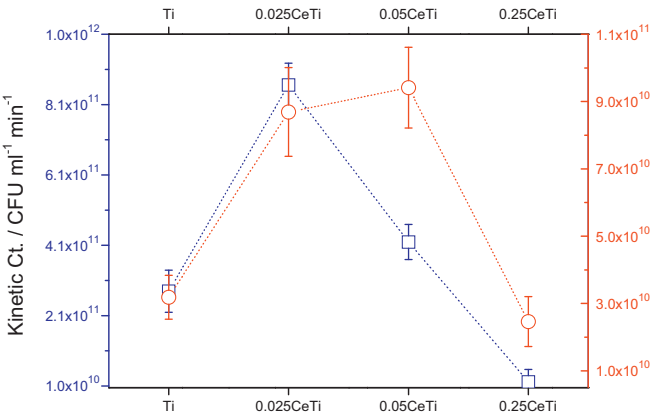

Fig. 7. Kinetic constants obtained from the kinetic analysis displayed in Fig. 4. Blue/Red color concerns UV/Visible results. (For interpretation of the color information in this figure legend, the reader is referred to the web version of the article.)

sample series for the UV case, the behavior of the corresponding series is mostly the one presented by the normalized reaction rates displayed in Fig. 1. The selectivity only modulates the behavior, providing a relatively smoother growth/decay up-to/from the maximum. The Q.E. enhancement factor of the 0.025CeTi samples with respect to the Ti reference is 4.7, to be compared with the 3.4 measured with reaction rates. For sunlight-type, the quantum efficiency shows (with respect to the surface-normalized rate) a smaller variation from the Ti reference to the 0.025CeTi samples but a larger variation on the decay part from the maximum at 0.05CeTi. Such maximum for the 0.05CeTi samples is similar in Figs. 2 and 5; enhancement factor are in this case 1.7 vs. 1.65, respectively, for surface-normalized rate and Q.E. The differential variation on the behavior of the two observables (surface-normalized rate and Q.E.) comes from the combined effect of the $e^{a,s}$ end selectivity changes, which cannot be predicted easily without the full calculation of the two variables. The main issue is that the rigorous calculation of the quantum efficiency demonstrates that the Ce-Ti composite system significantly improves photocatalytic performance with respect to the Ti (and Ce) reference materials by a factor which is 4.7 and 1.65 for, respectively, UV and Sunlight-type excitation. This occurs for different samples but having close Ce content.

Results of the photo-inactivation of *E. coli* are presented in Fig. 6. Note that blank experiments showed the absence of killing (less than 0.4 log CFU mL^{-1} at the end of the experiment) due to the very low irradiation power used in the experiments. Dark decays for xCeTi samples (not shown) were always below 0.7 log CFU mL^{-1}, indicating a relatively small contribution to the profiles displayed in Fig. 6. As a general description of the results, we observed, in agreement with previous results, a relatively high efficiency of the Ti reference system [18,19,41]. Significantly less activity is presented by the Ce single oxide reference. The xCeTi composite samples outperform the Ti reference for the 0.025CeTi and 0.05CeTi cases while the 0.25CeTi sample has similar (visible) or worse (UV) performance. We only are aware of a previous test concerning the biocidal potential of Ce-Ti composite systems. The experiments were done at dark conditions with rather high concentration(s) of the material at the liquid phase [49].

To interpret the disinfection capability of the samples, Fig. 6 also presents results for the modeling work. In the composite samples Ce can play a number of roles [5–7,41]. Modifying the interaction with the surface of the material can be the first. Surface roughness, hydrophobicity and net surface charge seem the most important surface variables to affect bacterial adhesion [71,72]. Note also that adhesion occurs in the experiments under light excitation, which modifies the hydrophobicity of the surface as a function of the light wavelength [73,74]. This explains the different interaction constants observed under UV and visible irradiation. The main issue is, however, the rough constancy of the interaction constant throughout the sample series up to the sample 0.25CeTi which may have a consistently larger value. The latter can be an effect related to the point of zero charge (also called isoelectric point, IE). An IE point near or above 7 (e.g., basic character) is required to have optimum *E. coli* inactivation [75]. Our titania has basis character [41] and ceria (or any other phase) is not expected to modify it significantly (modification below 15%) for loadings below 0.05% [76]. Thus, the detection of larger changes for the 0.25CeTi samples seems well justified on the basis of the mild basicity of ceria although their exact nature need to be further addressed. More importantly, for the most interesting *x*CeTi composite samples ($x = 0.025, 0.05$), lack of significant differences as to the initial contact with the bacteria can be noted with respect to the Ti reference.

The kinetic constant behavior through the sample series is presented in Fig. 7. The disinfection process occurred with significant activity both under visible and UV light excitations, albeit at much lower extent in the former. This fact is clearly reflected in the corresponding kinetic constant values plotted in Fig. 7. Values of the Ti reference are similar to previous ones (within 35%) although small differences in calcinations temperature (450 °C vs. 500 °C), wavelength (UV; from 280 to 350 nm) and fluence (small increase in the present case) can justify them [41]. In the case of the inactivation

Table 2
Kinetic analysis results from *E. coli* inactivation profiles presented in Fig. 1. *k*; kinetic constant; *K*, interaction constant; *n*; exponent coefficent.

Sample	k (min^{-1})	K (a.u)	n (a.u.)
UV; 350 nm			
Ti	31.7 (±1.5)	0.08_5 (±0.01)	1.12_5 (±0.07)
Ce	0.5 (±0.2)	0.10 (±0.02)	1.1 ($\pm 0.07_5$)
0.025CeTi	98.4 (±7.0)	0.12 (±0.05)	1.17 (±0.06)
0.05CeTi	47.6 (±4.0)	0.12 (±0.07)	1.14 (±0.08)
0.25CeTi	2.5 ($\pm 1.1_5$)	0.83 (±0.05)	1.08 (±0.07)
Visible; 500 nm			
Ti	3.6 ($\pm 0.7_5$)	1.5 (±0.2)	1.06_5 (±0.07)
Ce	0.4 ($\pm 0.1_5$)	1.7 (±0.2)	1.05_5 (±0.07)
0.025CeTi	9.9 (±1.5)	1.8 (±0.3)	1.13 (±0.08)
0.05CeTi	10.7 (±1.4)	1.6 (±0.3)	1.10 (±0.07)
0.25CeTi	2.8 (±0.8)	2.1 ($\pm 0.2_5$)	1.07(±0.07)

a.u.: adimensional units.

of *E. coli*, the enhancement factors with respect to the Ti reference are 3.1 (UV light; 0.025CeTi) and 3.0 (visible light; 0.05CeTi).

The similitude between results of Figs. 5 and 7 (elimination of toluene vs. inactivation of *E. coli*) is obvious, indicating a rather parallel behavior in terms of: (i) relative performance comparing UV and visible or sunlight-type excitations; and (ii) the shape of the curves and, particularly, the maxima obtained which, again, concern the 0.025CeTi samples for UV and 0.05CeTi for visible light. We thus observe that the photo-elimination process proceeds though the sample series in a similar way irrespective of the target nature, organic or biological, pointing out that the Ce-Ti system provides a powerful route to improve the properties of the Ti reference system.

Finally, to justify the inactivation curves it is therefore obvious that adhesion and charge carrier attack to the microorganism are important; however, other possible effects related to surface-poisoning need to be considered. The latter is quantified within our kinetic analysis by the inhibition coefficient (n) included in Table 2. This parameter accounts for the inhibition produced by the increasing concentration of cell debris and oxidation products appearing toward the end of the experiment and competing strongly for the radical species effectively eliminating microorganism [6,41,65]. The n coefficient is inherently higher than 1 and the larger the difference from this value the acute is the inhibition phenomenon. Table 2 shows relatively small differences (less than 7%) among samples for each excitation light. This suggests that the (differential; from *x*CeTi to Ti) influence of a self-poisoning effect in our disinfection tests is modest.

4. Conclusions

A series of five CeO_2-TiO_2 composite catalysts, with cerium loading in the 1–25 mol% range, were prepared by microemulsion using a single pot procedure and calcined at 500 °C. The catalysts are composed by nanoparticles of the two, ceria and anatase, oxides, and were characterized in terms of their morphological, structural and electronic properties in a previous publication [50].

In this contribution we applied kinetic schemes that open the playground for comparing quantitatively the relative performance of the CeO_2-TiO_2 composite samples with respect to the appropriate Ce and Ti single oxide references. Such an approach was used to interpret the photo-catalytic degradation of toluene as well as the inactivation of *E. coli*. In the case of the toluene mineralization we analyzed in detail the reaction by calculating the quantum efficiency and taking into account both the change in optical properties of the photo-catalysts as well as changes in the selectivity of the reaction. For the microorganism, the biocidal action of the photo-catalysts was measured in terms of the kinetic constants evolved from a simplified Langmuir-Hinshelwood-like reaction mechanism. From the results obtained we can conclude that low loaded Ce (below 0.05 mol%) composite samples outperforms nano-titania (including P25) reference systems by factors which are 4.7 (chemical depollution) and 3.1 (biological inactivation) under UV light, and 1.7 (chemical depollution) and 3.0 (biological inactivation) under sunlight-type or visible light excitation. The general improvement of activity no matter the excitation light energy and (chemical/biological) target nature would indicate that the Ce-Ti system can have potential to be a base system for future development of a broad-spectrum material in the field of photocatalysis.

Acknowledgements

A. Kubacka and M.J. Muñoz-Batista thank MINECO for support thought, respectively, the postdoctoral "Ramón y Cajal" and predoctoral FPI programs. Financial support by MINECO is also acknowledged (projects CTQ2010-14872/BQU and PRPPRI-PIBJP-2011-0914).

Appendix A. Calculation of the $e^{a,s}$ coefficient

A.1. Calculation of the $e^{a,s}$ coefficient

Gas phase photo-oxidation tests were carried out with toluene and using a set-up described in Fig. 8. Plots presented in Figs. 3 and 4 described the local rate of photon absorption; $e^{a,s}$, at the sample

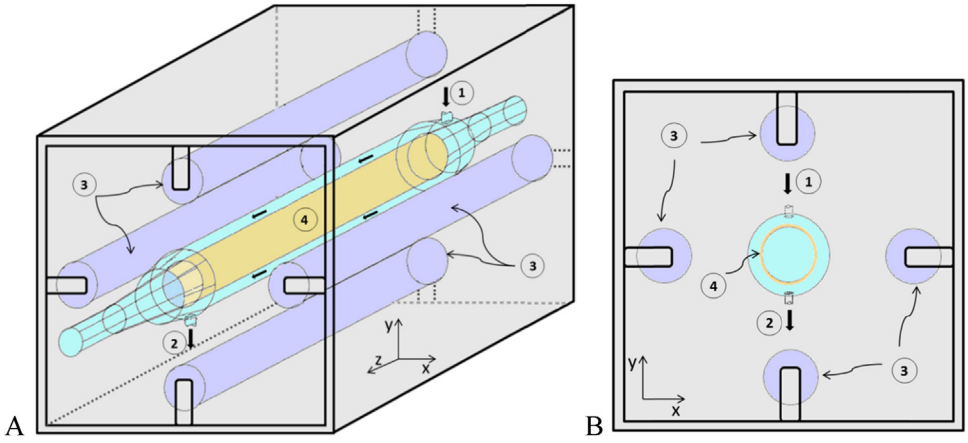

Fig. 8. (A) Photocatalytic annular reactor. (B) Side section view. (1) gas inlet, (2) gas outlet, (3) lamps, (4) catalyst sample.

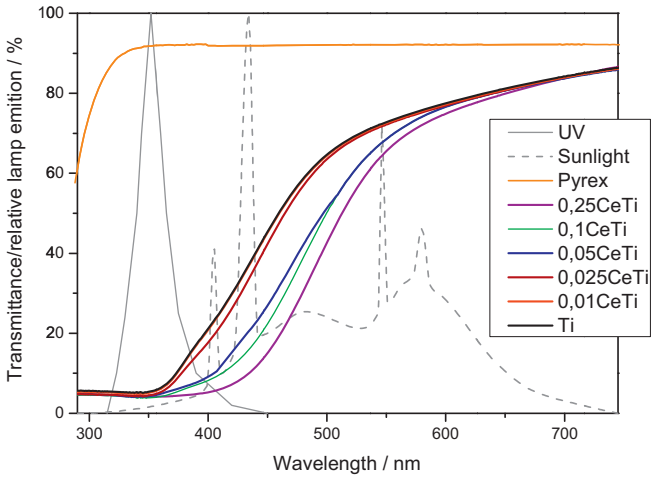

Fig. 9. Intensity distribution of the UV and sunlight-type lamps used in the photocatalytic experiments. For comparison the transmittance spectra of the pyrex reactor wall and samples are included.

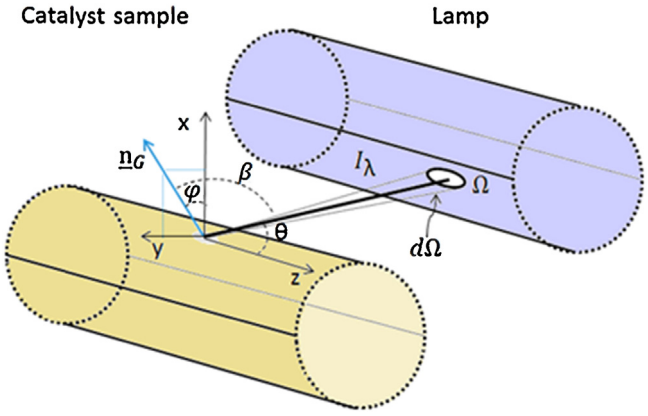

Fig. 10. Coordinate system used for equation A.1.

position *x,y,z* calculated using: (a) the annular reactor system described in Fig. 8; (b) the lamps intensity profiles presented in Fig. 9; and (c) the coordinate system described in Fig. 10. Such observable is obtained by addition of the contribution for each lamp according to the four-fold symmetry of the reactor system. The contribution of a single lamp follows the mathematical expression below described, which consider the interaction of the light with the two surfaces of the sample cylinder (see ref. 58 for details).

$$e_{\lambda}^{a,s}(x,y,z) =$$

$$\sum_{L=1}^{L=4}\sum_{\lambda}\int_{\varphi_{min}}^{\varphi_{max}}\int_{\varphi_{min}}^{\varphi_{max}} I_{\lambda,L}\times\exp\left(-\frac{K_{\lambda,g}e_g}{\cos\beta}\right)\left[1-\exp\left(-\frac{K_{\lambda,s}e_s}{\cos\beta}\right)\right]\sin^2\varphi[a(x)\cos\theta+$$

$$b(x)\sin\theta]\mathrm{d}\varphi\mathrm{d}\theta+\sum_{L=1}^{L=4}\sum_{\lambda}\int_{\varphi_{min}}^{\varphi_{max}}\int_{\varphi_{min}}^{\varphi_{max}} I_{\lambda,L}\times\exp\left(-\frac{2K_{\lambda,g}e_g-K_{\lambda,s}e_s}{\cos\beta}\right)[1- \quad (A.1)$$

$$\exp\left(\frac{K_{\lambda,s}e_s}{\cos\beta}\right)]\sin^2\varphi[a(x)\cos\theta+b(x)\sin\theta]\mathrm{d}\varphi\mathrm{d}\theta$$

Where

$$a(X)=\frac{X_S-X_L}{R};\ b(X)=\frac{X_S}{R} \quad (A.2)$$

Being *R* the radius of sample cylinder. The integration limits can be obtained using the following equations:

$$\varphi_{min}=\tan^{-1}\left(\frac{X_L-Xs_i}{Y_L-Ys_i}\right)-\sin^{-1}\left(\frac{RL}{(X_L-Xs_i)^2+(Y_L-Ys_i)^2}\right)$$

$$\varphi_{max}=\tan^{-1}\left(\frac{X_L-Xs_i}{Y_L-Ys_i}\right)-\sin^{-1}\left(\frac{RL}{(X_L-Xs_i)^2+(Y_L-Ys_i)^2}\right)$$

$$\theta_{min}(\varphi)=\cos^{-1}\frac{-Zs}{(X_{Lm}(\varphi)-Xs)^2+(Y_{Lm}(\varphi)-Ys_i)^2+Zs^2}$$

$$\theta_{max}(\varphi)=\cos^{-1}\frac{ZL-Zs}{(X_{Lm}(\varphi)-Xs)^2+(Y_{Lm}(\varphi)-Ys)^2+Zs^2}$$

Where:

$$X_{Lm}(\varphi)=X_L+(Xs-Y_L)\cos\varphi^2+(Y_L-Ys)(\cos\varphi\,\mathrm{sen}\varphi)$$
$$-\mathrm{sen}\varphi\sqrt{(RL^2-(Xs-X_L)\cos\varphi+(Y_L-Ys)\,\mathrm{sen}\varphi)^2)}$$

$$X_{Lm}(\varphi)=Ys+(Y_L-Ys)\cos\varphi^2+(Xs-Y_L)(\cos\varphi\,\mathrm{sen}\varphi)$$
$$-\cos\varphi\sqrt{(RL^2-(Xs-X_L)\cos\varphi+(Y_L-Ys)\,\mathrm{sen}\varphi)^2)}$$

References

[1] L. Jing, W. Zhou, G. Tian, H. Fu, Chem. Soc. Rev. 42 (2013) 9509–9549.
[2] V. Likodimos, C. Han, M. Peláez, A.G. Kontos, G. Liu, D. Zhu, S. Liao, S.P. Falaras, Ind. Eng. Chem. Res. 52 (2013) 13957–13964.
[3] M. Peláez, N.T. Nolan, S.C. Pillai, M.K. Severy, P. Falaras, A.G. Kontos, P.S.M. Dunlop, J.A. Bryne, D.D. Dionysiou, Appl. Catal. B 125 (2012) 331–349.
[4] A. Kubacka, G. Colón, M. Fernández-García, Chem. Rev. 112 (2012) 1555–1614.
[5] P.S.M. Dunlop, C.P.S. Sheeran, J.A. Bryne, M.A.S. McMahon, M.A. Boyle, K.G. McGuigan, J. Photochem. Photobiol. A 216 (2010) 303.
[6] O.K. Dalrymple, E. Stefanakos, M.A. Trozt, D.Y. Goswany, Appl. Catal. B 98 (2010) 27–65.
[7] M.A. Mahmood, S. Baruah, A.K. Anal, J. Dutta, Environ. Chem. Lett. 10 (2012) 1451–1459.
[8] M. Anpo, M. Takeuchi, J. Catal. 216 (2003), 505-318.
[9] A. Kubacka, M. Fernández-García, G. Colón, J. Catal. 254 (2008) 272–281.
[10] R. Asahi, T. Morikawa, T. Ohwaki, K. Aoki, Y. Taga, Science 293 (2001) 269–277.
[11] A. Kubacka, B. Bachiller-Baeza, B.G. Colón, M. Fernández-García, J. Phys. Chem. C 113 (2009) 8553–8556.
[12] A. Kubacka, B. Bachiller-Baeza, G. Colón, M. Fernández-García, Appl. Catal. B 93 (2010) 274–281.
[13] A. Kubacka, G. Colón, M. Fernández-García, Appl. Catal. B 95 (2010) 238–244.
[14] H. Gao, B. Lu, F. Liu, X. Shao, Int. J. Photoenergy (2012) 453018–453026.
[15] C.W. Lai, S. Sreekantan, J. Alloy Compd. 547 (2013) 43–50.
[16] J. Gou, et al., J. Appl. Phys. 114 (2013), no. 104803.
[17] W. Cao, M. Khan, J. Appl. Phys. 114 (2013) 183514.
[18] J.A. Rengifo-Herrera, K. Perzchala, A. Sienkiewicz, L. Forró, J. Kiwi, C. Pulgarin, Appl. Catal. B 88 (2009) 398–406.
[19] J.A. Rengifo-Herrera, C. Pulgarin, Solar Energy 84 (2010) 37–43.
[20] D. Robert, Catal. Today 122 (2007) 20–33.
[21] H.U. Lee, G. Lee, J.C. Park, Y.-C. Lee, S.M. Lee, B. Son, S.Y. Park, J. Lee, Chem. Eng. J. 240 (2014) 91–98.
[22] V. Augugliaro, L. Yurdakal, V. Loddo, G. Palmisano, L. Palmisano, Adv. Chem. Eng. 20 (2009) 1–35.
[23] G. Coló, n, S. Murcia López, M.C. Hidalgo, J.A. Navío, Chem. Commun. (2010) 4809–4811.
[24] M.J. Kim, K.-D. Kim, H.-D. Seo, Y. Luo, N.K. Dey, Y.D. Kim, Appl. Surf. Sci. 258 (2011) 2489–2499.
[25] N.K. Dey, M.J. Kim, K.-D. Kim, K.H. Lee, J. Mol. Catal. A 337 (2011) 33–38.

[26] R.G. Nair, J.K. Roy, S.K. Samdarshi, A.K. Mukherjee, Solar Eng. Mater. Solar Cells 105 (2012) 103–108.
[27] J. Tokarsky, V. Tatejka, L. Neuwirthova, J. Vontorova, J. Mamulova, K. Kutlakova, J. Kukutschova, P. Capkova, Chem. Eng. J. 222 (2013) 488–497.
[28] Q. Chen, C. Li, V. Paulinek, P. Sahara, H. Wang, Appl. Surf. Sci. 252 (2006) 4154.
[29] E. Pullido Melián, O. González Díaz, J.M. Doña Rodríguez, G. Colón, J.A. Navío, M. Macías, J. Pérez Peña, Appl. Catal. B 127 (2012) 112.
[30] M. Grandcolas, J. Ye, N. Hanagata, Mater. Lett. 65 (2001) 236.
[31] T. Sreethanwong, S. Ngansinlapasathian, S. Yoshida, Chem. Eng. J. 192 (2012) 292–300.
[32] S.A.K. Leghare, S. Sajjad, F. Chen, J. Zhang, Chem. Eng. J. 166 (2011) 906–915.
[33] C.W. Lai, S. Sreekantan, Int. J. Hydrogen Energy 38 (2013) 2156–2166.
[34] A. Kubacka, M.J. Muñoz-Batista, R. Rachwalik, B. Bachiller-Baeza, M. Fernández-García, J. Catal. 309 (2014) 428–438.
[35] M.K.I. Senevirathna, P.K.D.D.P. Pitigala, K. Tennakone, J. Photochem. Photobiol. A 171 (2005) 257.
[36] A. Torres, C. Ruales, C. Pulgarín, A. Aimable, P. Bowen, V. Sarria, J. Kiwi, ACS Mater. Interf. 2 (2010) 2547.
[37] C. Karunakaran, G. Abiramar, P. Gomathisankar, G. Manikandan, V. Anandi, J. Colloid Inter. Sci. 352 (2010) 68.
[38] D. Chen, H. Zhang, S. Hu, J. Li, J. Phys. Chem. C 112 (2008) 117.
[39] C. Karunakaran, G. Abiramar, P. Gomathisankar, G. Manikandan, V. Anandi, Mater. Res. Bull. 46 (2011) 1586.
[40] S.H. Hwang, J. Song, Y. Jung, O.Y. Kweon, H. Song, J.H. Jang, Chem. Comm. 47 (2011) 9164.
[41] A. Kubacka, M.J. Muñoz-Batista, M. Ferrer, M. Fernández-García, Appl. Catal. B 140–141 (2013) 680–690.
[42] M. Zou, Y. Kong, J. Wang, Q. Wang, Z. Wang, B. Wang, P. Fan, Spectrochim. Acta, Part A 101 (2013) 82–90.
[43] S. Parasupree, Y. Suzuki, S. Prisa-Art, S. Yoshikawa, S.J. Sol. St. Chem. 178 (2005) 128–134.
[44] G. Li, D. Zhang, Y.C. Yu, Phys. Chem. Chem. Phys. 11 (2009) 3775–3782.
[45] V. Stengl, S. Bakardejieva, N. Murafa, Mater. Chem. Phys. 114 (2009) 217–226.
[46] H. Lin, M. Wang, Y. Wang, Y. Liang, W. Cao, Y. Su, J. Photochem. Photobiol. A 223 (2011) 157–162.
[47] Y. Wang, B. Li, C. Zhang, L. Cui, S. Kang, X. Li, L. Zhou, Appl. Catal. B 130–131 (2013) 277–284.
[48] Y. Liu, P. Fang, Y. Cheng, Y. Gao, F. Chen, Z. Liu, Y. Dai, Chem. Eng. J. 219 (2013) 478–485.
[49] C. Karunakaran, P. Gomathisankar, ACS Sus. Chem. Eng. 1 (2013) 1555–1563.
[50] M.J. Muñoz-Batista, M.N. Gómez-Cerezo, A. Kubacka, D. Tudela, M. Fernández-García, ACS Catal. 4 (2014) 63–72.
[51] M.D. Hernández-Alonso, A.B. Hungría, A. Martínez-Arias, M. Fernández-García, J.M. Coronado, J.C. Conesa, J. Soria, Appl. Catal. B 50 (2004) 167–175.
[52] P. Ji, J. Zhang, F. Chen, M. Anpo, Appl. Catal. B 85 (2009) 148–154.
[53] G. Chen, J. Xiong, F.J. Stadler, Powder Technol. 249 (2013) 89–94.
[54] Y. Wang, F. Wang, Y. Chen, D. Zhang, B. Li, S. Kang, X. Li, L. Cui, Appl. Catal. B 147 (2014) 602–609.
[55] M. Fernández-García, A. Martínez-Arias, J.C. Hanson, J.A. Rodríguez, Chem. Rev. 104 (2004) 4063–4104.
[56] J. Marugán, R. Van Grieken, C. Pablos, M.L. Satuf, A.E. Cassano, O.M. Alfano, Appl. Catal. B 102 (2011) 404–416.
[57] O.M. Alfano, D. Bahnemann, A.E. Cassano, R. Dillet, R. Golisch, Catal. Today 58 (2000) 199–230.
[58] M.J. Muñoz-Batista, A. Kubacka, M.N. Gómez-Cerezo, D. Tudela, M. Fernández-García, Appl. Catal. B 140–141 (2013) 626–635.
[59] P.G. De Gennes, C. Taupin, J. Phys. Chem. 86 (1982) 2294–2303.
[60] M. Fernández-García, X. Wang, C. Belver, J.C. Hanson, J.A. Rodriguez, J. Phys. Chem. C 111 (2007) 674–682.
[61] B. Ohtani, Chem. Lett. 37 (2008) 167–189.
[62] M. Sleiman, P. Conchon, C. Ferronato, J.-M. Chovelon, Appl. Catal. B 86 (2009) 159–165.
[63] J. Sambrook, E.F. Fritsch, T. Maniatis, Molecular Cloning: A Laboratory Manual, second ed. Cold Spring Harbor: Cold Spring Harbor Laboratory Press, 1989.
[64] M. Ferrer, J. Soliveri, F.J. Plou, N. López-Cortés, D. Reyes-Duarte, M. Christensen, J.L. Copa-Patiño, A. Ballesteros, Enzyme Microb. Technol. 36 (2005) 391.
[65] J. Marugán, R. van Grieken, C. Sordo, C. Cruz, Appl. Catal. B 82 (2008) 27.
[66] J.E. Dennis, D.M. Gay, R.E. Welsh, ACM Trans. Math. Software 7 (1981) 348–369.
[67] D. Kotzias, Exp. Toxicol. Pathol. 57 (2005) 5–7.
[68] J. Mo, Y. Zhang, Q. Xu, Y. Zhu, J.J. Lamson, R. Zhao, Appl. Catal. B 89 (2009) 570–576.
[69] Y. Feng, L. Li, M. Ge, C. Gou, J. Wang, L. Liu, ACS Surf. Inter. 2 (2010) 3134–3140.
[70] L. Zhang, W.A. Anderson, Chem. Eng. J. 218 (2013) 247–252.
[71] C. Desrousseaux, V. Sautou, S. Descamps, O. Traoré, J. Hospital Inf. 85 (2013) 87–93.
[72] C. Pablos, R. van Grieken, J. Marugán, I. Chowdhury, S.L. Walker, Catal. Today 209 (2013) 140–146.
[73] B. Li, B.E. Logan, Colloid Surf. B 36 (2004) 81.
[74] N. J: Sucher, M.C. Carles, J. Nowotny, T. Bak, Adv. Appl. Ceram. 111 (2012) 16.
[75] D. Gumy, C. Morris, P. Bowen, C. Pulgarin, S. Giraldo, R. Hazdun, Kiwi, J. Appl. Catal. B 63 (2006) 76.
[76] A. Di Paola, E. García-López, G. Marci, C. Martin, L. Palmisano, V. Rives, A.M. Venezia, Appl. Catal. B 48 (2004) 223.